2018

# A new constitutive analysis of hexagonal close-packed metal in equal channel angular pressing by crystal plasticity finite element method

Hejie Li
*Tokyo Metropolitan University*, hejiel2003@gmail.com

Andreas Öchsner
*Griffith University*

Prasad K D V Yarlagadda
*Queensland University of Technology*

Yin Xiao
*Queensland University of Technology*

Tsuyoshi Furushima
*University of Tokyo*, tsuyoshi@uow.edu.au

*See next page for additional authors*

# A new constitutive analysis of hexagonal close-packed metal in equal channel angular pressing by crystal plasticity finite element method


## Abstract

Most of hexagonal close-packed (HCP) metals are lightweight metals. With the increasing application of light metal products, the production of light metal is increasingly attracting the attentions of researchers worldwide. To obtain a better understanding of the deformation mechanism of HCP metals (especially for Mg and its alloys), a new constitutive analysis was carried out based on previous research. In this study, combining the theories of strain gradient and continuum mechanics, the equal channel angular pressing process is analyzed and a HCP crystal plasticity constitutive model is developed especially for Mg and its alloys. The influence of elevated temperature on the deformation mechanism of the Mg alloy (slip and twin) is novelly introduced into a crystal plasticity constitutive model. The solution for the new developed constitutive model is established on the basis of the Lagrangian iterations and Newton Raphson simplification.





## Publication Details

Li, H., Ochsner, A., Yarlagadda, P. K. D. V., Xiao, Y., Furushima, T., Wei, D., Jiang, Z. & Manabe, K. (2018). A new constitutive analysis of hexagonal close-packed metal in equal channel angular pressing by crystal plasticity finite element method. Continuum Mechanics and Thermodynamics, 30 (1), 69-82.



## Authors

Hejie Li, Andreas Öchsner, Prasad K D V Yarlagadda, Yin Xiao, Tsuyoshi Furushima, Dongbin Wei, Zhengyi Jiang, and Kenichi Manabe

# A New Constitutive Analysis of Hexagonal Close-Packed Metal in Equal Channel Angular Pressing by Crystal Plasticity Finite Element Method

Hejie Li[1, 2, 4*], Andreas Öchsner[2, *], Prasad KDV Yarlagadda[3], Yin Xiao[4], Tsuyoshi Furushima[5], Dongbin Wei[6], Zhengyi Jiang[7], Ken-ichi Manabe[1, *]

[1]Department of Mechanical Engineering, Graduate School of Science and Engineering, Tokyo Metropolitan University, 1-1 Minami-osawa, Hachioji, Tokyo 192-0397, Japan

[2]Griffith School of Engineering, Griffith University Gold Coast Campus, Parklands Drive, Southport Queensland 4214, Australia

[3]School of Chemistry, Physics and Mechanical Engineering, Science and Engineering Faculty, Queensland University of Technology, 2, George Stret, Brisbane Qld 4001, Australia

[4] Institute of Health and Biomedical Innovation, & Science and Engineering Faculty, Queensland University of Technology, 60 Musk Avenue, Kelvin Grove, Brisbane, Queensland 4059, Australia

[5]Institute of Industrial Science, Department of Mechanical and Biofunctional Systems, the University of Tokyo, 4-6-1, Komaba, Meguro, Tokyo 153-8505, Japan

[6]School of Electrical, Mechanical and Mechatronic Systems, Faculty of Engineering and Information Technology, University of Technology, Sydney, NSW 2007, Australia

[7] School of School of Mechanical, Materials and Mechatronic Engineering, Faculty of Engineering and Information Sciences, University of Wollongong, Northfields Ave, Wollongong NSW 2522, Australia

**Key words:** Mg alloys, Slip, Twin, Temperature Effect, Constitutive Model

**Abstract:** Most of hexagonal close-packed (HCP) metals are lightweight metals. With the increasing application of light metal products, the production of light metal is increasingly attracting the attentions of researchers worldwide. To obtain a better understanding of the deformation mechanism of HCP metals (especially for Mg and its alloys), a new constitutive analysis was carried out based on previous research. In this study, combining the theories of strain gradient and continuum mechanics, the equal channel angular pressing (ECAP) process is analysed and a hcp crystal plasticity constitutive model is developed especially for Mg and its alloys. The influence of elevated temperature on the deformation mechanism of the Mg alloy (slip and twin) is novelly introduced into a crystal plasticity constitutive model. The solution for the new developed constitutive model is established on the basis of the Lagrangian iterations and Newton Raphson simplification.

# 1. Introduction

Currently, lightweight metals with excellent mechanical properties may bring a potential solution for the current energy crisis in automotive and aerospace industries. As one of the most promising lightweight metal, magnesium (Mg) is increasing the attentions of researchers and scientists in the world. Magnesium is the lightest structural metal. Generally, Mg has the following excellent properties: high corrosion resistance, low density, excellent impact resistance and damping capacity, and very good size stability (as shown in Figure 1) [1]. Magnesium alloys are mixtures of magnesium with other metals (called an alloy), often aluminum, zinc, manganese, silicon, copper, rare earths, and zirconium. Magnesium alloys have a hexagonal lattice structure, which affects the fundamental properties of these alloys. Plastic deformation of the hexagonal lattice is more complicated than in cubic latticed metals like aluminum, copper, and steel. Therefore, magnesium alloys are typically used as cast alloys, but research of wrought alloys has been more extensive since 2003. Cast magnesium alloys are used for many components of modern cars, and magnesium block engines have been used in some high-performance vehicles; die-cast magnesium is also used for camera bodies and components in lenses [2].

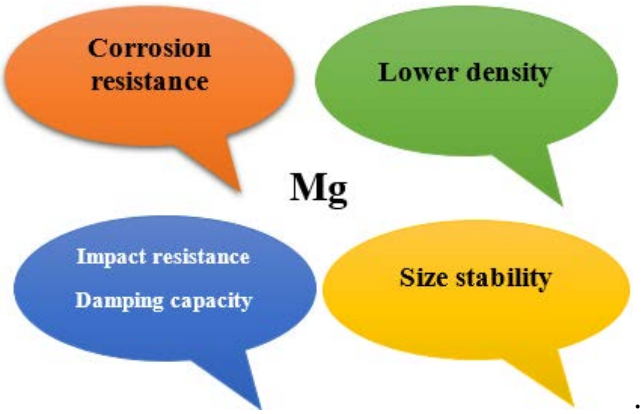


Figure 1: Characteristics of Mg [1]

Due to their low density and high specific strength, light metals - especially Mg alloys are becoming a hotspot of materials research not only in macro-forming, but also in micro-forming. The use of Mg alloy components is expanding, especially in the automotive industry, consumer electronics industry and medical industry [3, 4]. However, magnesium alloys have a HCP structure and the critical resolved stresses (CRSS) for a basal slip are far below that for non-basal slips [5]. Therefore, unlike other light metals such as aluminum, magnesium shows limited ambient temperature formability due to a shortage of independent deformation modes [6]. Due to a very poor workability and limited ductility at ambient temperature, most formings of Mg alloys are conducted at elevated temperatures, leading to a degradation of the mechanical properties (certain ductility, but low strength) [7, 8]. This makes the application of Mg alloy products very limited.

The significant disadvantages of Mg alloys are the poor workability and limited ductility at ambient

temperatures. The poor workability and ductility of Mg alloys mainly result from its limited slip system and special microstructure. In order to improve the workability and ductility of Mg alloys, many investigations have been conducted on the deformation mechanism of Mg and its alloys since the past several decades [9-17]. Mg alloys' deformation can be accommodated by slips on basal {0001}, prismatic $\{10\bar{1}1\}$ <a>, and pyramidal $\{11\bar{2}2\}$<c+a> planes. Deformation can also be accommodated by twining: tensile in $\{10\bar{1}2\}$ planes and contraction in $\{10\bar{1}1\}$ and $\{10\bar{1}3\}$ planes [18]. At room temperature, critical resolved shear stress (CRSS) associated with tensile twining in pure polycrystalline Mg and in conventional alloys such as Mg AZ31 alloy is slightly higher than the basal CRSS, but obviously lower than any non-basal CRSS (such as prismatic pyramidal <a> and pyramidal <c+a>). While compression twins are not common because the room temperature CRSS with this deformation mode is relatively higher than that of non-basal CRSS [17]. Some early investigations [10-12] showed that slips on basal planes and $\{10\bar{1}2\}$ twinning are the main deformation mechanisms during uniaxial deformation ate low temperature and low strain rate in randomly orientated Mg polycrystals of conventional grain size (10-50 μm). Non-basal slip systems are also active to a lesser extent [16, 19, 20]. High strain rate properties of metals and alloys were analyzed by Armstrong and Walley [21]. The strain rate response of metals depends on the crystalline structure [22]. For body-centered cubic (BCC) metals, the strain rate sensitivity coefficient reflects the yield stress dependence. For face-centered cubic (FCC) metals, the strain rated response of metals reflects strain hardening. In hexagonal close-packed (HCP) metals especially for Mg and its alloys with a random texture, the strain rate response follows the FCC pattern [23]. Simulation techniques aimed at describing the mechanical behavior of Mg alloys at quasi-static strain rates have been extensively proposed [9, 24-29]. Research also shows that the activity of Mg deformation mechanism is highly dependent on the temperature and initial texture [30, 31]. While the influence of temperature on the Mg deformation mechanism is not mentioned in details. Few research on the influence of temperature on the deformation behavior of HCP (Mg alloys) have been conducted in metal forming process especially for the case of ECAP. Therefore, to help the understanding of the deformation mechanism of Mg alloys in high temperature and also to provide suggestions on further optimization of mechanical properties of light metal (especially for Mg alloy), an analysis based on the constitutive model of Mg alloys at high temperature deformation has been carried out in this study on the basis of our previous research and analytical method of crystal plasticity constitutive model [32]. The influence of temperature on the strain increment is novelly employed in crystal plasticity finite element analysis of Micro ECAP process.

## 2. HCP material and its slip system

As a typical HCP metal, slip systems for Mg alloys includes two deformation mechanism: slip systems and twining systems. The sip system includes basal {0001}, prismatic $\{10\bar{1}1\}$ <a>, and pyramidal

$\{11\bar{2}2\}$<c+a> planes. While the twining consists of tensile in $\{10\bar{1}2\}$ planes and contraction in $\{10\bar{1}1\}$ and $\{10\bar{1}3\}$ planes. The typical deformation mechanism is show in Figure 2.

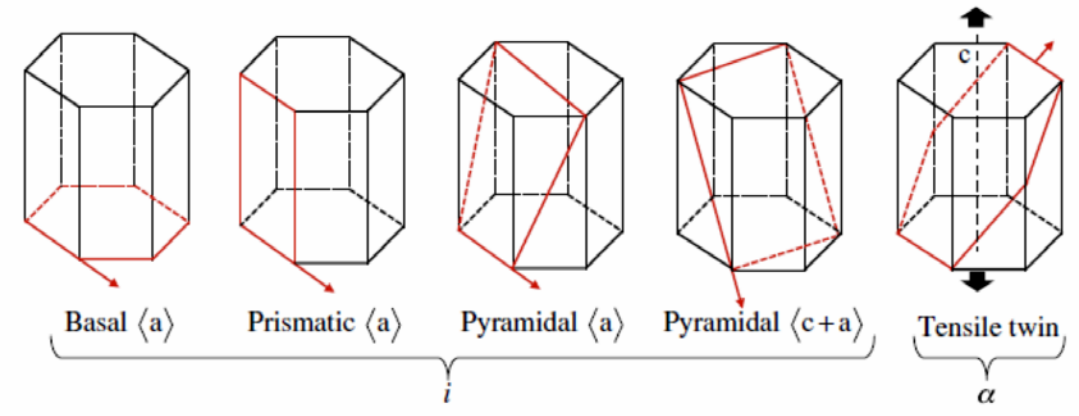


Figure 2 Schematic of the four hcp slip system (i) considered here, along with the tensile twinning system (a) [18]

## 3. ECAP system and deform mechanism

### 3.1 MECAP device

According to the requirement of the device, the ECAP device is developed based on the Japanese mechanical design standard, which is shown in Figure 3. Japanese steel SKD61 is used as the die material. The punch material is SKD 61 with nitriding treatment.

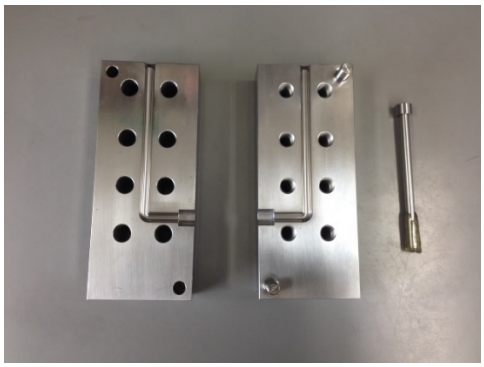

Figure 3 Micro-ECAP device: dies and punch

### 3.2 Deformation mechanism

The ECAP technology is a novel and high efficient manufacturing technology for bulk ultra-fined grain metal materials, whose mechanism is to obviously refine grains by the accumulation of severe shear deformation, then significantly improve the material property. In Figure 4(a), sever shear deformation will take place in the dotted line area. The effective strain can be accumulated due to an increase of the ECAP pass. In the ECAP process, the modelled sample evolution is shown in Figure 4 (b).

In the ECAP process, angles ϕ and ψ are the two important parameters, (as shown in Figure 4 (a)). Angle ϕ is the angle with the die between the two parts of the channel and angle ψ is the angle at the outer arc of the curvature at the point of intersection.

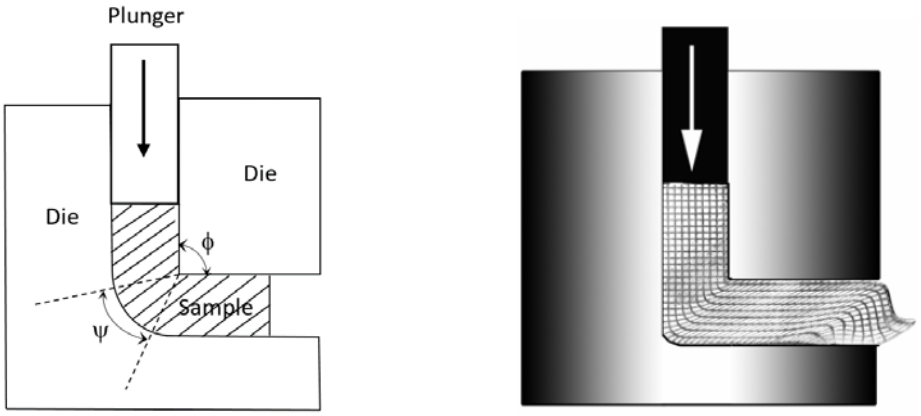


(a) (b)

Figure 4. Schematic of ECAP process: (a) ECAP device (die, punches and sample), (b) simulated sample deformation by FEM [33]

Figure 5 shows that a single pressing through the die shears the cubic element into a rhombohedra shape. However, it is also apparent that the deformation occurring in subsequent pressing will depend upon the nature of any rotation of the sample.

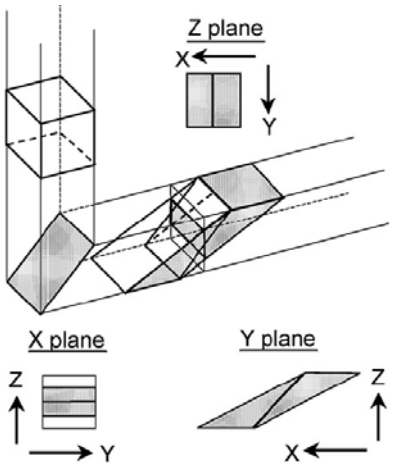


Figure 5. Schematic illustration of shearing in a single pressing through the die: X, Y and Z define orthogonal planes of observation [34]

### 3.3 ECAP pressure

As an important parameter, the ECAP pressure also plays an important role in workability, friction and even fatigue limit. Some researchers [35, 36] developed an upper-bound solution to the ECAP pressure considering Hollomon-type material and using a frictionless condition. According to these authors, the pressure is related with the material hardening behavior as [37-39]

$$P = \left(\frac{\sigma_y}{(n+1)}\right)\left[\frac{2\cot(\phi+\psi)/2)+\psi}{\sqrt{3}}\right]^{(n+1)} \quad (1)$$

Where $\sigma_y$ and $n$ are the yield stress and the strain-hardening exponent, respectively.

An analogue ECAP pressure solution considering a Swift-type material is based on

$$\sigma = \mathrm{K}(\varepsilon_0 + \varepsilon^p)^n \tag{2}$$

where *K* is the strength coefficient, $\varepsilon_0$ is the pre-strain and $\varepsilon^p$ is the effective von Mises plastic strain. Thus, considering one pass of extrusion the equation (1) becomes

$$\mathrm{P} = \left(\frac{K}{n+1}\right)\left\{\left(\frac{\sigma_y}{K}\right)^{\left(\frac{1}{n}\right)} + \left[\frac{2\cot((\phi+\psi)/2)+\psi}{\sqrt{3}}\right]^{(n+1)} - \left[\left(\frac{\sigma_y}{K}\right)^{\left(\frac{1}{n}\right)}\right]^{(n+1)}\right\} \tag{3}$$

The extrusion per unit of thickness after one pass can be obtained multiplying the right-hand side of the equation (3) by the width (W) of the billet. Thus

$$\frac{\mathrm{P}}{thickness} = \mathrm{W}\left(\frac{K}{n+1}\right)\left\{\left(\frac{\sigma_y}{K}\right)^{\left(\frac{1}{n}\right)} + \left[\frac{2\cot((\phi+\psi)/2)+\psi}{\sqrt{3}}\right]^{(n+1)} - \left[\left(\frac{\sigma_y}{K}\right)^{\left(\frac{1}{n}\right)}\right]^{(n+1)}\right\} \tag{4}$$

### 3.3 Strain in ECAP process

In the ECAP process, angles ϕ (the angle with the die between the two parts of the channel) and angle ψ (the angle at the outer arc of curvature at the point of intersection) are the important parameters which affect the ECAP strain greatly. Iwahashi et al. [40] studied the influence of the angle ψ on the ECAP deformation. They analyzed the results under three different conditions: A (ψ=0°), B (ψ=π−ϕ), C (0<ψ<π−ϕ). If the lubricant works well, the friction can be neglected. Under this condition, they proposed a relation between the effective strain and the ECAP angles ϕ and ψ. This expression is calculated from the von Mises isotropic yield criterion applied to the pure shear condition [40, 41].

$$\varepsilon_{eff} = \frac{1}{\sqrt{3}}\left[2\cot\left(\frac{\phi}{2}+\frac{\psi}{2}\right) + \Psi\cos\left(\frac{\phi}{2}+\frac{\psi}{2}\right)\right] \tag{5}$$

The effective strain $\varepsilon_{eff}$ in component form is represented by

$$\varepsilon_{eff} = \left[\frac{2\left(\varepsilon_x^2+\varepsilon_y^2+\varepsilon_z^2\right)+\left((\gamma_{xy}^2+\gamma_{yz}^2+\gamma_{zx}^2)/2\right)}{3}\right]^{1/2} \tag{6}$$

Since the same strain is accumulated in each passage through the die, the effective strain after *N* extrusion pass $\varepsilon_N$ may be expressed in a general from by the relationship

$$\varepsilon_N = N\cdot\varepsilon_{ef} = N\cdot\frac{1}{\sqrt{3}}\left[2\cot\left(\frac{\phi}{2}+\frac{\psi}{2}\right) + \Psi\cos\left(\frac{\phi}{2}+\frac{\psi}{2}\right)\right] \tag{7}$$

Thus, the strain may be estimated from this equation for any pressing condition provided the angles ϕ, ψ are known.

If the angle $\phi$ is 90°, the effective strain at different passes can be obtained as

Table 1 Effective strain at different passes

| Passes | 1 | 2 | 3 | 4 | 5 | 6 | 7 | 8 | 9 |
|---|---|---|---|---|---|---|---|---|---|
| Strain | 1.05 | 2.1 | 3.15 | 4.22 | 5.25 | 6.3 | 7.35 | 8.4 | 9.45 |

## 4. Constitutive relations of HCP metal

### 4.1 General assumptions in ECAP crystal plasticity finite element method simulation

Normally, finite element method simulations can provide direct information on the evolution of plastic deformation during the ECAP and enable us to simulate the deformation of the material subjected to single pass or multi-pass ECAP. Shaeri et al. [42] analysed the effect of the ECAP temperature on strengthening mechanisms of Al-Zn-Mg-Cu alloy and concluded that the ECAP temperature can strengthen the material by the following aspects: (i) solid solution hardening, (ii) grain boundary strengthening, (iii) dislocation strengthening and (iv) precipitation strengthening. However, these mechanisms will vary due to different metals and states. In the ECAP of Mg and its alloys, the strengthening will mainly be led by the second and third mechanism. To simplify the calculation, normally only the third strengthening mechanism will be taken into consideration in finite element modelling.

As a special approach of finite element method (FEM), crystal plasticity finite element modelling (CPFEM) can simulate the extra evolution of texture and surface profile. To simplify the simulation of CPFEM, some basic assumptions are needed. Based the two reasons, the general assumptions of the ECAP CPFEM can be summarized as follows:

(1) The material is isotopic and homogeneous.
(2) The material is elastic-plastic with the strain-hardening exponent being zero in order to consider the effect of elastic deformation on the morphological change of the extruded specimen.
(3) The system is isothermal.
(4) The von Mises flow rule is used to construct the constitutive relation.
(5) There is no friction between the surface of the material and the die wall due to the use of lubricant in the ECAP.
(6) The specimen volume is a constant during the ECAP process.
(7) Twin and slip are the main deformation modes. No other deformation mode take place in the ECAP process.
(8) In the same metal, all the slip systems have the same critical shearing stress;
(9) The trans-granular slip is homogenous.
(10) Influence of grain boundary is neglected.

Currently, this constitutive relationship does not consider the influence of dynamic recrystallization. For the other deformation, this model can be used by considering the practical deformation modes, temperature and the influence of dynamic recrystallization. With the consideration of deformation temperature and deformation modes, this model can be used in some hot deformation modes of Mg alloy such as hot rolling, hot extrusion etc. Different deformation modes have the different stress state: rolling has the stress state of 3 dimensional compression stress. While ECAP process, the shearing is the main deformation mode then shear force is the main force. The model should be modified by incorporating the different deformation mode (stress state) and other conditions (such as deformation temperature and lubrication), then it will be applicable for different deformation modes.

### 4.2 Thermodynamic and mechanics of geometry

The deformation gradient tensor $F$ at time $t$ can be decomposed multiplicatively into an elastic contribution $F_e$, related to the elastic distortion of the lattice, and a plastic contribution $F_p$, representing the cumulative effects of the non-reversible deformation in the crystal [43-47]:

$$\boldsymbol{F}(\mathrm{t}) = \boldsymbol{F}^{e}(t) \cdot \boldsymbol{F}^{p}(t) \tag{8}$$

Where det ($F^e$)>0 and det ($F^e$)=1 [26]

The stress is described by the second Piolar-Kirchoff tensor $S^e$ defined in the intermediary reference frame [48] which, in metals follows a linear relationship:

$$\boldsymbol{S}^{e} = \boldsymbol{C}\colon \boldsymbol{E}^{e} \tag{9}$$

Where $c$ is a fourth order anisotropic elasticity tensor, and $E^e$ is the elastic Green-Lagrange deformation tensor:

$$\boldsymbol{E}^{e} = \frac{1}{2}(\boldsymbol{C}^{e} - \boldsymbol{I}) \tag{10}$$

where $c^e$ is the elastic right Cauchy-Green tensor defined as

$$\boldsymbol{C}^{e} = \boldsymbol{F}^{eT} \cdot \boldsymbol{F}^{e} \tag{11}$$

Finally the plastic velocity gradient tensor $L^p = F^p \cdot \dot{F}^{p-1}$ is defined as [18]:

$$L^{p} = \sum_i sign(\tau_i)\dot{\gamma}_i \boldsymbol{S}_0^{i} + \sum_a sign(\tau_a)\dot{\gamma}_a \boldsymbol{S}_0^{a} \tag{12}$$

Where $\dot{\gamma}_i$ and $\dot{\gamma}_a$ are the shear strain rates and $s_0^i$ and $s_0^a$ are the Schmid tensors for slip system $i$ and twin system $\alpha$, respectively, in the reference configuration.

$$\begin{cases} \boldsymbol{S}_0^{i} = \boldsymbol{m}_0^{i} \otimes \boldsymbol{n}_0^{i} \\ \boldsymbol{S}_0^{\propto} = \boldsymbol{m}_0^{\propto} \otimes \boldsymbol{n}_0^{a} \end{cases} \tag{13}$$

Where $m_0^{i/\propto}$ and $n_0^{i/\propto}$ are the unit normal to the slip /twin plane, unit vector of the slip/twin direction in the reference configuration, respectively. A schematic of the corresponding systems is shown in Figure 2.

## 4.3 Incremental solution for simulation

### *4.3.1 Plastic deformation gradient increment*

The plastic deformation gradient tensor at time$\tau = \mathrm{t} + \Delta\mathrm{t}$, where $\Delta$t is the time step, can be given from its counterpart at time t, $F^p(t)$ by [25]

$$\boldsymbol{F}_p(\tau) = \boldsymbol{F}_{\Delta t}^{p} \cdot \boldsymbol{F}_p(\mathrm{t}) \tag{14}$$

Where $F_{\Delta t}^p$ is given by the kinematic incremental relation [25]:

$$F_{\Delta t}^{p} = 1 + \sum_i \Delta\gamma^{i}\, \boldsymbol{S}_0^{i} + \sum_a \Delta\gamma^{a}\, \boldsymbol{S}_0^{a} \tag{15}$$

Where $\Delta\gamma^i$ and $\Delta\gamma^a$ are the shear strain increment.

### *4.3.2 Influence of temperature on strain increment*

Normally, the relationship between the temperature and the strain rate can be expressed [49] as

$$\dot{\varepsilon} = A\left(\frac{\sigma}{G}\right)^n \left(\frac{D_0}{b^2}\right)\exp\left(-\frac{Q}{RT}\right) \quad (16)$$

Where $A$ is a constant, σ is the flow stress, $D_0$ is the pre-exponential factor for diffusion, $G$ is the shear modulus, $n$ is the stress exponent (=1/m), $b$ is Burgers vector, $R$ is the gas constant, $T$ is the absolute temperature (K) and $Q$ is the activation energy for diffusion, which depends on the rate controlling process. Ishikawa et al. [50] analysed the influence of temperature on the ECAP deformation of AZ31 Mg alloy. From their results, they obtained the value of stress exponent $n$ and $m$: $n$=5-7, and $m$=0.14-0.2. Based on their results and research of Robinson and Sherby [51, 52], the practical diffusion coefficient of $D$ can be obtained by the following equation.

$$\mathrm{D}_{eff} = D_L + u(\sigma/G)^2 D_P \quad (17)$$

Where $\mathrm{D}_{eff}$ is the effective diffusion coefficient, $D_L$ is the lattice diffusion coefficient, $D_P$ is the pipe diffusion coefficient and $u$ is a constant and is generally considered to be 7.4 [52].

If the influence of the ECAP temperature on deformation mechanism is taken into consideration, the slip shear increment is shown as

$$\Delta\gamma_S^i = \Delta\gamma_P^i + \Delta\gamma_H^i \quad (18)$$

Where $\Delta\gamma_p^i$ and $\Delta\gamma_H^i$ are the slip shear increment led by the deformation and temperature, respectively.

$$\Delta\gamma_H^i = K_p T + A_0 \quad (19)$$

Where $K_p$ is the temperature coefficient, which has an obvious effect on the deformation of slip, $T$ is the pressing temperature, K, $A_0$ is a constant, which is depend on the pressing temperature in the ECAP process.

In the ECAP process, the twin shear increment is shown as

$$\Delta\gamma_T^a = \Delta\gamma_P^a + \Delta\gamma_H^a \quad (20)$$

Where $\Delta\gamma_p^a$ and $\Delta\gamma_H^a$ are the twin shear increment led by the deformation and temperature respectively. $T$ is the pressing temperature, $K$, $B_0$ *i*s a constant which is depend on the pressing temperature in the ECAP process.

$$\Delta\gamma_H^a = K_a T + B_0 \quad (21)$$

Where $K_a$ is the temperature coefficient, which has an obvious effect on the formation of twining, $T$ is the pressing temperature, $K$, $A_0$ is a constant.

### *4.3.3 Volume of slip and twin on strain increment*

Main deformation mechanism of HCP metal includes two deformation system. In this study, it was then assumed that except slip and deformation twin, there is no other deformation mechanism. Therefore the

plastic deformation volume can only be divided into two parts: slip and deformation twin (in this case, compression twin is the main twin system).

$$V_p = V_S + V_T \tag{22}$$

Where $V_p$ is the total plastic deformation volume, as assumed it is 1, $V_S$ is the deformation volume led by the slip (less than 1), $V_T$ is the deformation volume resulted from the deformation twin (less than 1).

For each strain increment $\tau$, the plastic deformation volume can be expressed as

$$V_{p,\tau} = V_{S,\tau} + V_{T,\tau} \tag{23}$$

The Where $V_{p,\tau}$ is the total plastic deformation volume at the strain increment $\tau$, as assumed it is 1, $V_{S,\tau}$ is the deformation volume led by the slip (less than 1) at the strain increment $\tau$, $V_{T,\tau}$ is the deformation volume resulted from the deformation twin (less than 1) at the strain increment $\tau$.

### 4.4 Critical resolved shear stress

Therefore, the resolved shear stresses (RSSs) for all slip systems *i* and twin systems $\alpha$ are defined as [18]

$$\begin{cases} \tau_i = (\boldsymbol{C}^e : \boldsymbol{S}^e) \cdot \boldsymbol{S}_0^i \\ \tau_\alpha = (\boldsymbol{C}^e : \boldsymbol{S}^e) \cdot \boldsymbol{S}_0^a \end{cases} \tag{24}$$

At the initial time *t*, all the variables ($\boldsymbol{F}(\mathrm{t})$, $\boldsymbol{F}_p(\mathrm{t})$, $\boldsymbol{S}^e(t)$, $\boldsymbol{S}_0^i(t)$ *and* $\boldsymbol{S}_0^a(t)$ ) are all known. But at time increment Δt, only $\boldsymbol{F}(\mathrm{t})$is available. For simplification of the calculation, a set of trial values are defined for the calculation of other variables. Therefore, for all the other incremental variables can be calculated by the following setting and equations.

$$\begin{cases} F^e(\Delta t)^{tr} = F(\Delta t) \cdot F^p(t)^{-1} \\ \boldsymbol{C}^e(\Delta t)^{tr} = F^{eT}(\Delta t)^{tr} \cdot F^e(\Delta t)^{tr} \\ E^e(\Delta t)^{tr} = \frac{1}{2}(\boldsymbol{C}^e(\Delta t)^{tr} - I) \\ S^e(\Delta t)^{tr} = \boldsymbol{C} : E^e(\Delta t)^{\tau r} \end{cases} \tag{25}$$

Therefore at time $\tau$ ($\tau$=$\Delta t$), the RSSs for slip systems *i* and twin system $\alpha$ in equation (18) can be expressed by trial values as

$$\begin{cases} \tau_i(\Delta t)^{tr} = S^e(\Delta t)^{tr} \cdot \boldsymbol{S}_0^i(t) \\ \tau_\alpha(\Delta t)^{tr} = S^e(\Delta t)^{tr} \cdot \boldsymbol{S}_0^a(t) \end{cases} \tag{26}$$

With an assumption of $sign(\tau_i(\Delta t)^{tr}) = sign(\tau_i(\Delta t))$ (for slip systems) and $sign(\tau_\alpha(\Delta t)^{tr}) = sign(\tau_\alpha(\Delta t))$ (for twin systems), the RSSs for slip systems and twin systems can be obtained as follows:

The RSSs for slip systems:

$$|\tau_i(\Delta t)^{tr}| = |\tau_i(\Delta t)| + \sum_{i,j \in N} \left\{ sign(\tau_i(\Delta t)^{tr}) sign\left(\tau_j(\Delta t)^{tr}\right) \boldsymbol{S}_0^i(t) : \boldsymbol{C} : [sym(\boldsymbol{C}^e(\Delta t)^{tr} \cdot \boldsymbol{S}_0^i(t))] \right\} \Delta\gamma_j \tag{27}$$

Where *N* is the set of activated systems in the grains, *i* and *j* are the activated slip systems, respectively.

The RSSs for twin systems:

$$|\tau_\alpha(\Delta t)^{tr}| = |\tau_\alpha(\Delta t)| + \sum_{\alpha,\beta \in N} \left\{ sign(\tau_\alpha(\Delta t)^{tr}) sign\left(\tau_\beta(\Delta t)^{tr}\right) \boldsymbol{S}_0^\alpha(t) : \boldsymbol{C} : [sym(\boldsymbol{C}^e(\Delta t)^{tr} \cdot \boldsymbol{S}_0^\alpha(t))] \right\} \Delta\gamma_\beta$$

(28)

Where $N$ is the set of activated systems in the grains, $\alpha$ and $\beta$ are the activated slip systems respectively.

Normally in crystal plasticity finite element modelling, four slip systems and one twin system are employed: Basal <a> ($\{0001\}<11\bar{2}0>$), prismatic <a> ($\{1\bar{1}00\}<11\bar{2}0>$), pyramidal <a> ($\{1\bar{1}00\}<11\bar{2}0>$), pyramidal <c+a> ($\{11\bar{2}2\}<\bar{1}\bar{1}23>$) and tensile twin <c> ($\{10\bar{1}2\}<\bar{1}011>$, contraction (compression) twin in <c> $\{10\bar{1}1\}$ and $\{30\bar{3}4\}$ planes [53-55]. Due to the different deformation mechanism and deformation plane, the slip and twin of HCP metal can be judged by the critical resolution saturation stress and the deformation plane. In this case, deformation twin is the main twin system. For materials with five hexagonal crystal symmetry, five independent elastic constants of pure Mg were used in the present work [56]: $C_{11}$=58GPa, $C_{12}$=25GPa, $C_{13}$=20.8GPa, $C_{33}$=61.2GPa, $C_{55}$=16.6GPa. In the theoretical simulation, reference values of all the parameters are list in Table 2.

Table 2 The parameters of microscopic hardening coefficient used in the CPFEM is as [57]

| Mode | $\tau_0^{\alpha}$ (MPa) | $h_0$ (MPa) | $\tau_{sat}$ (MPa) | α |
|---|---|---|---|---|
| Basal<a> | 25 | 100 | 70 | 1.1 |
| Prism<a> | 68 | 130 | 210 | 0.8 |
| Pyram<a> | 68 | 130 | 210 | 0.8 |
| Pyram<c+a> | 68 | 130 | 210 | 0.8 |
| Twin | 40 | 50 | 50 | 1.1 |

### 4.4 Strain rate dependency law

In rate dependent formulations [58-61], the consistency condition is accomplished by establishing a relation between slip/twin rates and the corresponding instantaneous RSSs. In this work the shear rate deformation on slip/twin systems is given by the following power law flow rule [60]:

$$\dot{\gamma_i} = \begin{cases} \dot{\gamma}_0 \left[ \left( \frac{\tau_i}{s_i} \right)^{\frac{1}{m_i}} - 1 \right] & if\ \tau_i \geq s_i \\ 0 & otherwise \end{cases} \tag{29}$$

Where for each system $i$, $s_i$ is the CRSS, $\dot{\gamma_i^0}$ the reference shear rate and $m_i$ the strain rate sensitivity coefficient. As a consequence, a system is considered activated when $\dot{\gamma}_i$>0, i.e. when $\Delta\gamma_i$>0. As noted by several authors [62, 63], the previous equation is slightly different from the one proposed by Cuition and Ortiz [60]. In this equation, the initial yielding is shifted to mitigate the tendency of the original model proposed by Hutchinson [58] to predict unrealistic values of sear rate. Additionally, this shifted relation is also numerically more stable.

Along with the incremental hardening relationship,

$$s_i(\Delta t) = s_i(t) + \left(\sum_{j \in N} h_{i,j}(t)\, \Delta\gamma_i\right) \Delta s_i \tag{30}$$

Where $h_{i,j}$ is the hardening matrix at time $t$.

According to Garcia-Grajales et al. [18] research, the trial RSSs for twin system can be represented as:

$$\sum_{\alpha,\beta\in N}\left\{sign(\tau_\alpha(\Delta t)^{tr})sign\left(\tau_\beta(\Delta t)^{tr}\right)\boldsymbol{S}_0^\alpha(t):\boldsymbol{C}:\left[sym\left(\boldsymbol{C}^e(\Delta t)^{tr}\cdot\boldsymbol{S}_0^\alpha(t)\right)\right]+h_{\alpha,\beta}(t)\left(\frac{\Delta\gamma_i}{\Delta t\dot{\gamma}_\alpha^0}+1\right)^{m_\alpha}\right\}\Delta\gamma_\beta =$$

$$|\tau_\alpha(\Delta t)^{tr}|-s_a(\mathrm{t})\left(\frac{\Delta\gamma_i}{\Delta t\dot{\gamma}_\alpha^0}+1\right)^{m_\alpha} \quad (31)$$

The slip systems are the same just by replacing $\alpha$ and $\beta$ with $i$, $j$ in equation (29). At each time step, the consistency condition leads to a system of nonlinear equations which is opposed to the rate independent formulation [9].

### 4.5. Implicit resolution

Normally, solutions for CPFEM includes two parts: the explicit solution (dynamic state) and the implicit solution (static state). In our study, the implicit solution will be implemented because most cases focus on the metal forming process with very low deformation speed (strain rate).

Define A and B are the matrix and right hand side corresponding to the RI formulation. For the twin system, the two parameters can be defined as follows:

$$\begin{cases}A_{\alpha,\beta}=sign(\tau_\alpha(\Delta t)^{tr})sign\left(\tau_\beta(\Delta t)^{tr}\right)\boldsymbol{S}_0^\alpha(t):\boldsymbol{C}:\left[sym\left(\boldsymbol{C}^e(\Delta t)^{tr}\cdot\boldsymbol{S}_0^\alpha(t)\right)\right]+h_{\alpha,\beta}(t)\\ B_a=|\tau_\alpha(\Delta t)^{tr}|-s_a(\mathrm{t})\end{cases} \quad (32)$$

Therefore, equation (31) can be simplified as

$$\begin{cases}A(\Delta\gamma)\cdot\Delta\gamma=b(\Delta\gamma)\\ \Delta\gamma_\beta\geq 0,\forall\beta\in N\end{cases} \quad (33)$$

From equation (20) the

$$\Delta\gamma_\beta=\Delta\gamma_P+\Delta\gamma_H \quad (34)$$

Where $\Delta\gamma_P$is the twin increment led by plastic deformation, $\Delta\gamma_H$is the twin increment led by the ECAP temperature.

Therefore, equation (33) can be rewritten as

$$\begin{cases}A(\Delta\gamma)\cdot\Delta\gamma=b(\Delta\gamma)\\ \Delta\gamma_\beta=\Delta\gamma_P+\Delta\gamma_H\\ \Delta\gamma_\beta\geq 0,\forall\beta\in N\\ \Delta\gamma_P\geq 0,\ \forall P\in N\\ \Delta\gamma_H\geq 0,\forall H\in N\end{cases} \quad (35)$$

Equation (33) can be numerically solved by use of the Newton-Raphson method with line search and backtracking strategies [64]. Following this method, the function to minimise is defined as follows:

$$f_a\left(\Delta\gamma_\beta\right)=A_{\alpha,\beta}\left(\Delta\gamma_\beta\right)\Delta\gamma_\beta-B_a\left(\Delta\gamma_\beta\right) \quad (36)$$

The numerical approximation of the Jacobian (i.e.,$J_{\alpha,\beta} = \frac{df_\alpha}{d\Delta\gamma_\beta} \approx \frac{\delta f_\alpha}{\delta\Delta\gamma_\beta}$, $\forall\alpha,\beta \in N$ was used for the Newton-Raphson algorithm as it was shown to offer more stability than the analytical evaluation. Therefore, equation (36) can be expressed as

$$J_{\alpha,\beta} = A_{\alpha,\beta}(\Delta\gamma_\beta) - \frac{B_\alpha(\Delta\gamma_\beta)}{\Delta\gamma_\beta}, \forall\alpha, \beta\in\mathrm{N} \tag{37}$$

### 4.6 Flow chart of HCP metal UMAT code

Based on previous research [65], the flow chart of the UMAT code of the HCP metal (Mg alloy) can be developed for the application in the commercial finite element package ABAQUS. The flow chart in this theoretical simulation is shown in Figure 6.

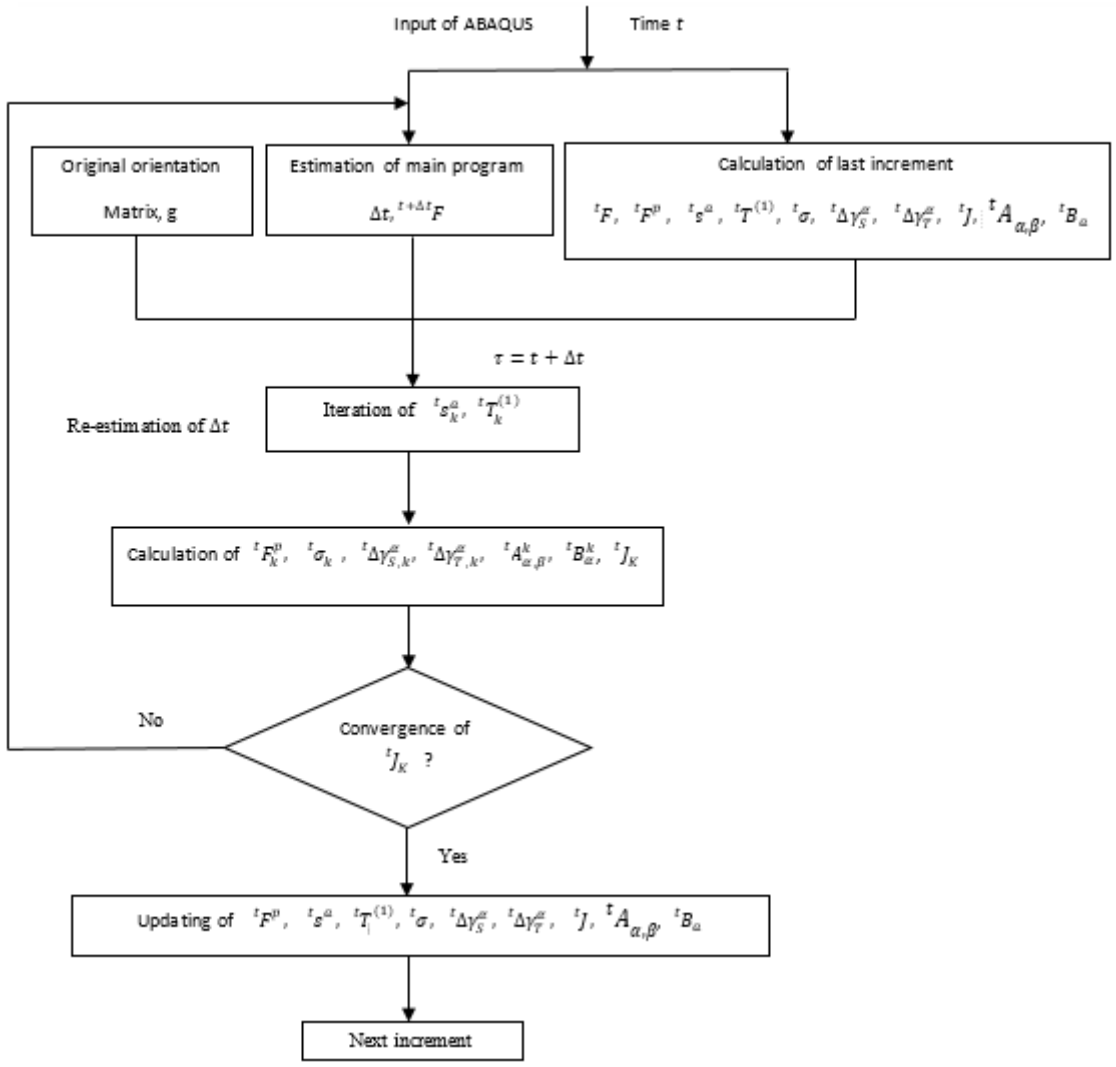


Figure 6 Flowchart of the UMAT code of HCP metal (Mg alloy) used in ABAQUS

When the UMAT is first used, the increment step will be initialised and the data of grain orientation and slip system will be input. At a starting time *t* of the incremental step, the ABAQUS main program will input UMAT with the initial grain orientation matrix, time increment, and all the updating variables calculated from the last step. Then the variables ${}^{\tau}s_k^{\alpha}$ and ${}^{\tau}T_k^{(1)}$ of time $\tau$ will be iterated and solved. The values of variables ${}^{\tau}F_k^{p}$, ${}^{\tau}\sigma_k^{\alpha}$, ${}^{\tau}\Delta\gamma_{S,k}^{\alpha}$, ${}^{\tau}\Delta\gamma_{T,k}^{\alpha}$, ${}^{\tau}A_{\alpha,\beta}^{k}$, ${}^{\tau}B_{\alpha}^{k}$, ${}^{\tau}T_k^{(1)}$, and the Jacobian matrix ${}^{\tau}J_k$ can be obtained by the related equations. If the Jacobian matrix converges, the values of ${}^{\tau}F^{p}$, ${}^{\tau}s^{\alpha}$, ${}^{\tau}T^{(1)}$, ${}^{\tau}\sigma^{\alpha}$, ${}^{\tau}\Delta\gamma_S^{\alpha}$, ${}^{\tau}\Delta\gamma_T^{\alpha}$, ${}^{\tau}A_{\alpha,\beta}$, ${}^{\tau}B_{\alpha}$ and ${}^{\tau}J$ will be updated, and then the iteration of the next increment will be calculated. If the Jacobian matrix does not converge, the time increment will be estimated and iterated. The Newton-Raphson iteration method is used in ABAQUS to solve the non-linear finite element equilibrium equation. It is as [65-68]

$$\sum\left(\int M^T J M dV\right) C^K = P(t+\Delta t) - \sum\int M^T[\sigma(t) + \Delta\sigma(\Delta u^k)]dV \tag{38}$$

$$\Delta u^{k+1} = \Delta u^k + C^k \tag{39}$$

where *M* is the transfer matrix from the dislocation increment to the strain increment, $\Delta\varepsilon = M\Delta u$. The stress increment is a function of the strain increment and a function of the dislocation increment. After the K times' iteration, the corrected displacement is given in the first equation. When the Newton-Raphson iterating method is used to solve the finite element equations, the Jacobian matrix ${}^{t+\Delta t}J = {}^{t+\Delta t}\left(\partial\Delta\sigma/\partial\Delta\varepsilon\right)$ (matrix DDSDDE) will be updated. If the Jacobian matrix cannot be expressed explicitly, the rigid matrix can replace it. In the solving process, the time increment and deformation gradient of time *t* is input into the UMAT by the ABAQUS program and the increment of stress tensors will be updated, and the stress tensor at time $t+\Delta t$ will be obtained. If the Jacobian matrix can be expressed implicitly, the matrix DDSDDE needs to be updated to improve the rate of convergence.

## 5. Conclusions

In this study, a new crystal finite element model for a HCP metal (Mg and its alloys) in the ECAP process was established by employing the traditional crystal plastic constitutive equations. The influence of the ECAP temperature on deformation mechanism is firstly introduced into the crystal plasticity constitutive model. With this optimized model, much more accurate prediction can be made in the ECAP process especially in the case involving high temperature states. The new model will be improved by the practical test by optimizing the values of parameters. It also has a potential application in other high temperature metal forming process of Mg and Mg alloys.

## Acknowledgements

The first author will show his heart-felt thanks to JSPS for providing the financial support to complete the manuscript writing and equation deduction and analysis. Thanks will be also given to Tokyo Metropolitan University and Professor Ken-ichi Manabe for providing working space and other related working resources for this manuscript.

**References**

[1] M.P. Staiger, A.M. Pietak J. Huadmai, G. Dias, Biomateiral, 27(2006), 1728-1734.

[2] G.Y. Yuan, X.B. Zhang, J.L. Niu, H.R. Tao, D.Y. Chen, Y.H. He, Y. Jiang, W.J. Ding. The Chinese Journal of Nonferrous Metals, 21(10), 2011, 2476-2488.

[3] E. Aghion, B. Bronfin. Mater Sci. For, 350-351(2000), 19-30

[4] B.L. MroDIKE, T. Ebert, Mater. Sci. and Eng., A, 302(2001), 37-45

[5] J. Hirsch, T.Al-Samman. Acta Mater., 61(2013) 818-843

[6] T. Mayama, M. Noda, R. Chiba, M. Kuroda. In. J. of Plas., 27(2011), 1916-1935

[7] H.E. Friedrich, B.L. Mordike, Magnesium Technology, Springer, New York, 2006

[8] F. Czerwinski, Magnesium Injection Molding, Springer, New York, 2008

[9] A. Fernandez, M.T. Perez-Prado, Y. Wei, A. Jerusalem, Int. J. Plast. 27(2011),1739-1757.

[10] S.L. Couling, J.F. Pashak, L. Sturkey, Trans. Am. Soc. Met. 51(1959),94-107.

[11] U.F. Kocks, D.G. Westlake, Trans. Metall. Soc AIME 239 (1967), 1107-1109.

[12] G.Y. Chin, W.L. Mammel, Metall. Trans. 1(1970) 357-361.

[13] S.S. Vagaralia, T.G. Langdon, Acta Metall. 29(12) (1981), 1969-1982.

[14] J.W. Christian, S Mahajan, Prog. Mater Sci. 39(1-2) (1995), 1-157.

[15] S.R. Agnew, M.H. Yoo, C.N. Tome, Atca Mater. 49(20) (2001), 4277-4289.

[16] S.R. Agnew, O. Duygulu, Int. J. Plast. 21(6) (2005), 1161-1193.

[17] A. Chapuis, J.H. Driver, Acta Mater. 59(2011), 1986-1994.

[18] J.A. Garcia-Grajales, A. Fernandez, D. Leary, A. Jerusalem. Comput. Mater. Sci., 115(2016), 41-50

[19] J. Koike, T. Kobayashi, T. Mukai, H. Watanabe, M.Suzuki, K. Maruyama, K. Higashi, Acta Mater. 51(7) (2003), 2055-206.

[20] Z. Keshavarz, M.R. Barnett, Scripta Mater. 55(10) (2006), 915-918.

[21] R.W. Armstrong, S.M. Walley, Int. Mater. Rev. 53(3) (2008), 105-128.

[22] A. Serra, D.J. Bacon, Mater. Sci. Eng., A400-401 (2005), 496-498.

[23] B.A. Bilby, A.G. Crocker, Proc. Roy. Soc. 288 (1965), 240-255.

[24] A. Fernandez, A. Jerusalem, I. Gutierrez-Urrutia, M.T. Perez-Prado, Acta Mater. 61(2013), 7679-7692.

[25] A.V. Staroselsky, L. Crystal Plasticity due to slip and twining (Ph. D thesis), Massachusetts Institute of Technology, 1998.

[26] A.V. Staroselsky, L. Anand Int. J. Plast, 19(10), (2003), 1843-1864.

[27] J. levesque, K. Inal, K.W. Neale, R.K. Mishra, Int. J. Plast. 26(2010), 65-83.

[28] V. Herrerz-Solaza, J. LLorca, E. Dogan, I. Karaman, J. Segurado, Int. J. Plast. 57(2014), 1-15.

[29] P. A. Juan, S. Berbenni, M.R. Barnett, C.N. Tome, L. Capolungo, Int. J. Plast. 60(2014), 182-196.

[30] R. Gehrmann, M.M. Frommert, G. Gottstein, Mater. Sci. Eng., A 395(1-2) (2005), 338-349.

[31] T. Al-samman, G. Gottstein, Mater. Eng., A 488(1-2) (2008), 406-414.

[32] H.J. Li, A. Öchsner, G.W. Ni, D.B. Wei, Z.Y. Jiang, Continuum Mech Therm, 28(6) (2016), 1623-1634.

[33] C.W. Jens. Equal Channel Angular Pressing (ECAP) of AA6082: Mechanical Properties, Texture and Microstructural Development, Ph. D thesis, Norwegian University of Science and Technology (NTNU), 2004, 17.

[34] A. Azushima, R.Kopp, A.Korhonen, D.Y. Yang, F. Micari, G.D. Lahoti, P. Groche, J. Yanagimoto, N. Rosochowski, A. YAnangida, CIRP-Manufacturing Technology, 57 (2008) 716-735.

[35] M.L. Alexander V.P. Alexander, A.K Panayiotis, N.A. Konstantinos, A.E. Yuri, 8th International Conference “Research and Development in Mechanical Industry”, 2008, 236-240. (Uzice, Serbia)

[36] M.L. Alexander, V.P. Alexander, A.K. Panayiotis, International Conference on Computational plasticity, 2009, 1-4 (Barcelona, Spain)

[37] R. Melicher, Applied and Computational Mechanics, 3(2009), 319-330.

[38] R Melicher, M. Handrik, Acta Mechanica Slovaca, 3-C/2008, Kosice, 2008, 273-284. (in Slovak)

[39] R. Melicher, Finite element method simulation of equal channel angular pressing, In Transcom 2009, Zilina, 2009, 91-94.

[40] Y. Iwahashi, J. Wang, Z. Horita, et al. Scripta Mater, 3(1996),143.

[41] R. Melicher, Applied and Computational Mechanics, 3(2009), 319-330

[42] M.H. Shaeri, M. Shaeri, M. Ebrahimi, M.T. Salehi, S.H. Seyyedein, Progress in Natural Science: Materials International, 26(2016), 182-191.

[43] E. Kroner, On the plastic deformation of polycrystals, Acta Mater., 9 (1961), 155-161.

[44] E. Kroner, Kontinuumstheorie der Versetzungen und Eigenspannungen. Berlin: Springer, (1958) (in German).

[45] E. Kroner, In: Physics of defects. Amsterdam, Netherlands: North-Holland Publishing Company. (1981).

[46] E. Kroner, Allgemeine Kontinuumstheorie der Versetzungen und Eigenspannungen, Arch Ration Mech Anal., Vol. 4 (1959), 273-334.

[47] E.H. Lee, and D.T. Liu, Finite-strain elastic-plastic theory with application to plane-wave analysis, J Appl Phys., 38 (1967), 19-27.

[48] L. Malvern, Introduction to the Mechanics of a Continuum Medium, Prentice-Hall, 1969.

[49] C.R. Barret, A.J. Ardell, O.D. Sherby, Trans AIME 230 (1964), 200.

[50] K. Ishikawa, H. Watanabe, J. Mater. Sci., 40(2005), 1577-1582.

[51] S.L. Robinson, O.D. Sherby, ibid, 17(1969), 109.

[52] O.A. Ruano, J. Wadsworth, O.D. Sherby, J. Mater. Sci. 20(1985), 3735.

[53] R.E. Reed-Hill, W.D. Robertson, Acta Metall. 5(12) (1957), 717-727.

[54] R.E. Reed-Hill, W.D. Robertson, Acta Metall. 5(12) (1957), 728-737.

[55] H. Yoshinaga, T. Obara, S. Morozumi, Mater. Sci. Eng. 12(5-6), 255-264

[56] G. Simmons, H. Wang, Single crystal elastic constants and calculated aggregate properties: a handbook, Cambridge, (MA): MIT Press; 1971.

[57] S.H. Choi, D.H. Kim, S.S. Park, B.S. You, Acta Mater, 58(2010), 320-329.

[58] J.W. Hutchinson, Proc. Roy. Soc. London, 348(1976), 101-127.

[59] R.J. Asaro, A. Needleman, Acta Metall. 33(1985), 923-953.

[60] A.M. Cuitino, M. Ortiz, Modell. Simul. Mater. Sci. Eng. 1(1992), 225-263.

[61] Z. Zhao, S.N. Kuchnicki, R.A. Radovitzky, A.M.C Cuitino, Acta Mater. 55(2007), 2361-2373.

[62] X. Ling, M.F. Horstemeyer, G.P. Potirniche, Int. Numer. Meth. Eng. 63(2005), 548-568.

[63] R.D. Mcginty, D.L. Mcdowell, Int. J. Plast. 22(2006) 996-1025.

[64] W.H. Press, Numerical Recipes for Fortran 77. Cambridge University Press, 1992.

[65] H.J. Li, Surface roughness in metal forming, Ph. D thesis, University of Wollongong, 2012.

[66] ABAQUS/Standard user's manual. Hibbitt, Karlsson& Sorensen, Inc, (2002).

[67] SIMULINK, ABAQUS GUI Toolkit Reference Manual, USA, (2008).

[68] Z. Zhuang, F. Zhang, and S. Cen. Analysis and examples of ABAQUS Nonlinear Finite Element. Beijing: Science Press (2004).